EEET ECOLOGICAL ENGINEERING & ENVIRONMENTAL TECHNOLOGY

Ecological Engineering & Environmental Technology, 2025, 26(10), 205–217
https://doi.org/10.12912/27197050/210952
ISSN 2719–7050, License CC-BY 4.0

Received: 2025.08.14
Accepted: 2025.09.15
Published: 2025.10.01

Adsorptive elimination of methyl orange from aqueous systems employing biochar derived from Malus domestica waste

Fikri Nabil[1*], Youssef Hattafi[1], Lamyae Mardi[2], Lahcen Benaabidate[1], Abderrahim Lahrach[1]

[1] Laboratory of Geo-Resources and Environment, Faculty of Science and Technology, Sidi Mohamed Ben Abdellah University, BP Imouzer Road, Fez 30500, Morocco
[2] Laboratory of Materials, Process, Catalysis and Environment, Higher School of Technology, Sidi Mohamed Ben Abdellah University, Fes, Morocco
* Corresponding author's e-mail: fikrinabil59@gmail.com

ABSTRACT

This study investigates the valorization of Malus domestica debris from the Ifrane region of Morocco for the production of H_3PO_4 activated biochar and its application in the elimination of methyl orange (MO**)** from aqueous solutions via batch adsorption. A comprehensive characterization of the activated biochar was conducted using specific surface area analysis, Boehm titration, point of zero charge (pHpzc) determination, thermogravimetric analysis (TGA) and X-ray diffraction (XRD) measurements. The findings indicate that phosphoric acid activation enhances both the specific surface area and functional group density of the biochar. Kinetic and equilibrium models were used to assess the adsorption process, and the Freundlich, Langmuir, and Temkin isotherms were fitted to the equilibrium data. The results demonstrate that adsorption capacity rises with time until equilibrium is attained following ninety minutes of contact. In addition, phosphoric acid activation enhanced the quantity of MO adsorbed per gram of biochar. Under optimized conditions, equilibrium adsorption kinetics followed a pseudo-second-order model, while the Langmuir isotherm provided the best fit for describing MO adsorption, with a maximum adsorption capacity of 143.65 $mg \cdot g^{-1}$. Thermodynamic analysis revealed that the adsorption process is endothermic and primarily governed by physical interactions. These findings highlight the potential of H_3PO_4 activated biochar derived from Malus domestica debris as a highly effective and sustainable adsorbent for the removal of methyl orange from aqueous solutions.

Keywords: biomass valorization, adsorption, waste water treatment, waste management.

INTRODUCTION

The toxicity and non-biodegradable characteristics of organic pollutants make them a serious environmental hazard. Among these contaminants, synthetic dyes are particularly concerning, as they are widely present in industrial effluents from the dyeing, textile, leather, paper, and plastics industries (Lellis et al., 2019). These dyes are extremely visible and unattractive even at very low concentrations, and they pose harmful, mutagenic, carcinogenic, and allergic concerns to human health and ecosystems (Sudarshan et al., 2023). Several conventional methods have been devised for the treatment of industrial wastewater polluted with dyes, including coagulation/flocculation, chemical oxidation, membrane filtration, electrodialysis, and ozonation (Dutta et al., 2021). However, these techniques are often economically unfeasible and suffer from significant drawbacks, including the generation of hazardous residues or by-products that require further management or treatment, excessive reagent and energy consumption, and inadequate dye removal (Iwuozor et al., 2021).

However, adsorption has become a popular and successful technique for removing dyes from wastewater. Compared to traditional treatment methods, adsorption offers several advantages, including operational adaptability, ease

of implementation and design, minimal sludge generation, and relatively low setup costs (Ighalo et al., 2022). Activated biochar, in particular, has been extensively utilized as an adsorbent due to its high adsorption capacity, which stems from its favorable physical and chemical properties (Biswal and Balasubramanian, 2023).

This study aims to explore the removal of methyl orange (MO) from aqueous solutions through adsorption onto biochar derived from the chemical activation of *Malus domestica* debris collected from Ifrane, Morocco. The biochars were prepared using phosphoric acid (H_3PO_4) at different impregnation ratios (40%, 70%, and 100% by mass). The physicochemical characteristics of the biochars were analyzed through Boehm titration for surface chemistry, point of zero charge (pHpzc) measurements, and thermogravimetric analysis. The pore structure was characterized using methylene blue (MB) adsorption and iodine index measurements. The adsorption behavior of MO was examined using Langmuir, Freundlich, and Temkin isotherm models, while adsorption kinetics were evaluated and modeled using the pseudo-first-order, pseudo-second-order, and intraparticle diffusion equations.

MATERIALS AND METHODS

The colorant used is Methyl Orange, an anionic (acidic) dye classified within the aminoazobenzene family. It functions as a color indicator, specifically helianthine, and is extensively utilized in chemical applications. The physicochemical characteristics of MO are detailed in Table 1, and solutions were prepared using distilled water.

Table 1. Physico-chemical characteristics of methyl orange

Parameter	Methyl orange
Chemical names	4-benzenesulfonic acid (acid form) 4-sodium benzene sulfonate (sodium salt)
Color index	CI orange acide 52
Chemical formula	$C_{14}H_{14}N_3O_3SNa$
Maximum wavelength λ_{max}	463
Logarithmic acidity constant pK_a^b	3.30
Water solubility at 20°C ($g{\cdot}L^{-1}$)	5.20
Molecular size	14.38 x 6.56 x 4.04

Preparation and characterization of the biochars

Apple tree (Malus Domestica) debris harvested in the locality of Dayet Aoua (Ifrane region, Morocco), was used as a raw material for the manufacture of biochars. After being manually crushed in a mortar and sieved to produce particles smaller than 600 µm in diameter, they were repeatedly cleaned with distilled water to get rid of contaminants and dried for 48 hours at 50 °C in an oven. This aggregate (20 g) was impregnated with a given mass of phosphoric acid (H_3PO_4) in aqueous solution (60 mL) for 4 h at 20 °C to form a slip. Impregnation ratios were varied in the following range: 40%, 70% and 100%, X_{imp} expressed as a mass percentage being 100 times the ratio of the mass of H_3PO_4 to the mass of precursor (100 x m_{H3PO4} [g]/$m_{MalusDomestica}$[g]), in order to obtain biochars of different porosity. The suspensions were then evaporated in an oven at 110 °C for 24 h. The impregnated and dried samples were then activated for 2 h at 500 °C in a pyrolysis oven (heating rate: 15 °C·min^{-1}) under ambient air. The biochars were cleaned in a glass funnel with boiling distilled water to get rid of any remaining phosphoric acid. Using a $Pb(NO_3)_2$ lead nitrate test (0.1 mol·L^{-1}), washing was done until no phosphate ions were left in the water. Following three hours of drying at 110 °C, the recovered material was crushed and sieved to produce particles with a diameter of less than 75 µm. Biochars (ABs) prepared with X_{imp} = 40%, 70% and 100% were named AB40, AB70 and AB100 respectively. Several methods have been used to characterize our activated biochars. The iodine value provides information on the micropore surfaces (internal surfaces) accessible to small molecules and metals. The average iodine uptake (mg/g) of each biochar sample was determined using the following equation:

$$Iodine\ index\ (mg.g^{-1}) = \frac{\left[C_0 - \frac{C_n V_n}{2V_{I_2}}\right] M_{I_2} V_{Ads}}{m_{AB}} \quad (1)$$

where: C_0 is the original iodine solution's concentration (0.1 mol·L^{-1}), Cn: is the sodium thiosulfate solution's concentration (mol·L-1), V_n – the volume of sodium thiosulfate solution at equivalence (mL), V_{I2}: iodine solution dosage volume (10 mL), V_{ads}: the volume of iodine solution adsorbed (20 mL), M_{I2} – the molecular weight of iodine (254 g·mol^{-1}) and *mAB*: the mass of biochar (g).

Boehm titration (selective neutralization) was used to determine the contents of oxygenated and basic groups. pH measurements were performed using a pH meter.

Determination of zero charge point pH was carried to identify the surface charge of the activated biochars (AB30, AB60, AB100). The experiment to determine the pH_{pzc} of each adsorbent begins by preparing 40 mL of 0.1 M $NaNO_3$ in ten separate Erlenmeyer flasks. The pH values of these solutions are adjusted across a range from 2 to 12 using either 0.1 M HCl or NaOH, monitored with a pH meter. Then, 0.15 g of biochar is added to each flask, and the mixtures are shaken at 150 rpm on an orbital shaker at 30 °C for 24 hours to reach equilibrium. After equilibrium, the contents are filtered, and the final pH values of the filtrates are recorded (Candamano et al., 2023). The point of zero charge (pH_{pzc}) is determined graphically by plotting the final pH (pH_{final}) against the initial pH ($pH_{initial}$), and identifying where the curve intersects the line $pH_{final} = pH_{initial}$ (El Alouani et al., 2018).

Thermogravimetric analysis (TGA) was employed to study how mass changes and heat flow occur with changes in temperature in a controlled environment. This analytical method is commonly used to investigate processes like evaporation, combustion characteristics and thermal decomposition (Fikri et al., 2025). Specifically, in this study, we conducted TGA analysis using an STA (TG) Thermogravimetric Analyzer. We heated the sample at a rate of 5.00 °C per minute until reaching 900 °C, with air flowing through the system (Saadatkhah et al., 2020).

XRD analysis was performed using an X'Pert PRO diffractometer (Cu-Kα radiation), scanning over a range of 2θ angles to characterize the crystalline structure of the samples.

Nitrogen adsorption–desorption analyses (3P Instruments GmbH & Co. KG) were employed to determine the Brunauer-Emmett-Teller (BET) surface area, pore volume, and pore size distribution. The specific surface area of the activated biochars was calculated using the methylene blue index by the Equation 2 and the specific surface area of the sample occupied by the MB molecule (S_{MB}) using the Equation 3:

$$\frac{C_e}{Q_e} = \frac{1}{K_L Q_{max}} + \frac{C_e}{Q_{max}} \tag{2}$$

$$S_{MB} = Q_{max} A_{MB} \left(\frac{6.02\ x\ 10^{23}}{M_{MB}} \right) \tag{3}$$

where: C_e – residual solution concentration at adsorption equilibrium (mg·L^{-1}), Q_e – The quantity of adsorbate adsorbed at equilibrium (mg·g^{-1}), K_L: adsorption equilibrium constant for the Langmuir solute/adsorbent pair (L·mg^{-1}) and Q_{max}: The highest amount adsorbed (mg·g^{-1}), MB: molecular surface area (A_{MB}) of 1.30 nm^2 and a molar mass (M_{MB}) of 319.85g.mol^{-1} (Hang and Brindley,1970).

Batch adsorption

Adsorption was studied in batch (stirred tank) in Erlenmeyer flasks stirred at 300 tr·min^{-1}, at room temperature (25 °C) and at pH of the reaction medium equal to 4 for MO and 6 for MB. After separation of the liquid phase and adsorbent by filtration through glass microfiber filters (1 µm pores), the evolution of filtrate concentration at different contact times was monitored using a UV–visible spectrophotometer at a wavelength of 460 nm for MO (Table 1) and 665 nm for MB. Calculation of the adsorbed quantity is given by Equation 4:

$$Q_e = \frac{(C_0 - C_e)\, V}{M} \tag{4}$$

where: C_0 and C_e are respectively the initial and equilibrium concentrations (mg·L^{-1}), m is the mass of the adsorbent (g) and V the volume of solute (L).

MO adsorption kinetics were studied at the initial concentration of 20 mg·L^{-1} in contact with a biochar mass of 0.05 g (experimental conditions: solution volume = 50 mL; T = 25 °C; stirring speed = 300 tr·min^{-1}). Adsorption isotherms were obtained for a quantity of biochars of 0.05 g by varying the MO and MB concentration between 20 and 300 mg·L^{-1}. At pH 4 and 6, respectively, adsorption isotherms were examined in closed Erlenmeyer flasks with 50 mL of MO or MB solution at 25 °C while being stirred at 300 tr·min1. To guarantee that an adsorption equilibrium was established, the contact time was chosen at 24 hours. The amount of MO (or MB) adsorbed at equilibrium (Q_e), expressed in mg·g^{-1}, was calculated by Equation 4. The linear transforms of the Langmuir, Freundlich and Temkin adsorption isotherm models are derived from Equations 2, 6 and 7. The dimensionless separation factor R_L is calculated using the Equation 5:

$$R_L = \frac{1}{1 + K_L C_0} \tag{5}$$

$$\log Q_t = \log K_f + n \log C_e \quad (6)$$

$$Q_e = BlnA + BlnC_e \quad (7)$$

where: K_L is the adsorption equilibrium constant for the Langmuir solute/adsorbent pair ($L \cdot mg^{-1}$), C_0 is the initial concentration ($mg \cdot L^{-1}$), K_f and n are Freundlich constants that characterize the efficiency of an adsorbent with respect to a given solute.

The adsorption kinetics of methyl orange by biochar were examined using pseudo-first order (Equation 8), pseudo second order (Equation 9), and intraparticle diffusion (Equation 10) models.

$$log(Q_e - Q_t) = log\, Q_e - \frac{K_1}{2.303} t \quad (8)$$

$$\frac{t}{Q_t} = \frac{1}{K_2 Q_e^2} + \frac{1}{Q_e} \quad (9)$$

$$Q_t = K_{int} t^{1/2} + C \quad (10)$$

where: K_1 (min^{-1}) is the pseudo-first-order constant, K_2 ($g \cdot mg^{-1} \cdot min^{-1}$) is pseudo-second-order constant, K_{int} ($mg \cdot g^{-1} \cdot min^{1/2}$) intraparticle diffusion constant; Qt – is the capacity for adsorption at time t and Q_e – is the equilibrium adsorption capacity.

Thermodynamic parameters, such as adsorption enthalpy (ΔH_T), adsorption entropy (ΔS_T) and adsorption free energy (Gibbs energy: ΔG_T), were determined using the following Equations 11, 12 and 13:

$$lnK_L = \frac{\Delta S_T}{R} - \frac{\Delta H_T}{RT} \quad (11)$$

$$K_L = {Q_e}/{C_e} \quad (12)$$

$$\Delta G_T = -RTlnK_L \quad (13)$$

where: K_L is Langmuir's constant ($L \cdot g^{-1}$); T is the temperature in K and R the universal gas constant: 8.314 $J \cdot mol^{-1} \cdot K^{-1}$.

RESULTS AND DISCUSSION

Production yield

Thermochemical activation yields for biochars ranged from 56.7 for 40% impregnation to 37.4% for 100% impregnation. These yields indicate that the decomposition of organic matter increases significantly with the rise in the phosphoric acid (Ximp) impregnation. The decrease in yield from 56.7 to 37.4% with increasing impregnation ratio from 40 to 100% is attributed to increased carbon combustion by excess H_3PO_4, leading to enlargement of micropores into mesopores. The impregnation process using 70% phosphoric acid results in a yield of 48.2%.

Characterization of biochars

The specific surface area (S_{MB}) values determined from methylene blue adsorption isotherms were 320, 561 and 618 $m^2 \cdot g^{-1}$ for AB40, AB70 and AB100 respectively.

The specific surface area of the adsorbents increases as the chemical activation ratio rises. Furthermore, the specific surface area obtained through the iodine test follows the trend AB40 > AB70 > AB100 and increases with phosphoric acid concentration, as reported in the literature (Zeng et al., 2021). The specific surface areas of the activated biochars studied were compared with those of other materials from the bibliography. The results show that the surface areas of biochars synthesized in this study significantly exceed those of many previously reported biochars. For instance, biochar derived from corncob exhibited a much lower surface area of only 56.91 m^2/g (Shao et al., 2018), while untreated pine sawdust biochar had a moderate surface area of 168 m^2/g (Chu et al., 2018). Similarly, untreated oak wood biochar reached 231.15 m^2/g (Kim et al., 2019), whereas chemically activated biochars showed higher values. Biochar from nori activated with $ZnCl_2$ exhibited a surface area of 294.2 m^2/g (Wang et al., 2020), and lignocellulosic biochar activated with carbon dioxide achieved 316 $m^2.g^{-1}$ (Kozyatnyk et al., 2021). In contrast, the activated biochars in this study, particularly AB70 and AB100, displayed superior surface areas, emphasizing the effectiveness of the activation process applied here.

According to Table 2, the percentage of oxygenated functional groups in the chemically prepared adsorbent increases with increasing impregnating agent concentration. For AB40, AB70 and AB100, the percentages of oxygenated functional groups are 6.7%, 8.6% and 7.2% respectively. These values exceed those obtained for biochar produced from date palm waste (Usman et al., 2015). Indeed, the generation of oxygen or sulfur functional groups on an adsorbent surface

Table 2. Chemical surface properties of the activated biochars

Surface chemical characteristics	Activated Biochars		
	AB40	AB70	AB100
Phenolic groups (mEq.g^{-1})	0.007	0.009	0.0014
Carboxylic groups (mEq.g^{-1})	0.002	0.004	0.006
Total oxygen groups (mEq.g^{-1})	0.009	0.013	0.0153
Total basic groups (mEq.g^{-1})	0.0064	0.0012	0.036
Oxygenated functional groups (%)	6.7	8.6	7.2
Specific surface area S_{MB} ($m^2.g^{-1}$)	320.41	560.71	618.48
Iodine index (mg. g^{-1})	296.48	317.34	362.71
pH_{pzc}	6.52	6.81	7.23

can enhance adsorption properties by enhancing the number of available sites (Dai et al., 2021).

Boehm titrations of ABs obtained from 40%, 70% and 100% impregnation ratios (Table 2) show fewer basic groups than acidic groups (carboxylic and phenolic groups), confirming their slightly acidic character.

The pH_{pzc} values of the adsorbents are listed in Table 2. Cation adsorption on all adsorbents will be favorable at pH values above pH_{pzc}, while anion adsorption will be favored at pH values below pH_{pzc}. This is due to the fact that, at a pH below pH_{pzc}, the biochar surface is protonated (acidic) and positively charged. On the other hand, at a pH above pH_{pzc}, the biochar surface is deprotonated (basic):it is negatively charged.

Following chemical activation, pH_{pzc} increases progressively and in proportion to the activation rate, from 6 (raw biochar) to 6.52, 6.81and 7.23 respectively for AB40, AB70, and AB100. The TGA curves for the biochars (ABs) as shown in Figure 1, reveal an initial mass loss occurring below 300 °C, which is attributed to the desorption of bound water, specifically water that is physiosorbed in microspores and mesopores. The mass losses recorded for impregnation ratios of 40%, 70%, and 100% are 12.26%, 14.43%, and 16.12%, respectively. Notably, biochar AB40 exhibits a mass loss of only 12.26%, indicating its lower hydrophilicity, as it contains fewer surface oxygen groups compared to AB70 and AB100, along with a higher proportion of basic groups relative to these latter biochars. These observations corroborate the results previously reported by (Boumanchar et al., 2017).The second phase of mass loss, observed on the plateau between 300 °C and 600 °C, can be interpreted as the decomposition of surface oxygen groups. The mass

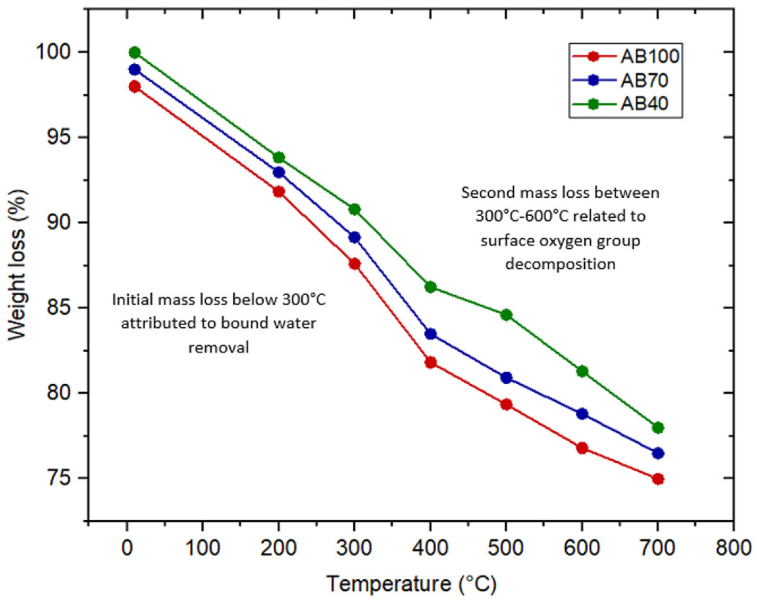

Figure 1. Thermogravimetric analysis of activated biochars (AB40, AB70, AB100)

losses during this temperature range are 6.44%, 8.76%, and 7.08% for AB40, AB70, and AB100, respectively. The relatively low mass loss of 6.44% for biochar AB40 is consistent with its lower content of oxygenated functional groups, quantified at 0.009 mEq·g^{-1}, alongside its higher concentration of basic functional groups. These observations corroborate with results reported by (Premchand et al., 2024).

The XRD diffraction patterns of the raw and activated biochars is presented in Figure 2. The observed peaks at approximately 2θ = 26° and 2θ = 37° correspond to the presence of insoluble $CaCO_3$ and SiO_2 crystals on the biochar surface (Jiang et al., 2024). A peak around 2θ = 43° indicates the formation of more stable carbon structures following activation (Alcazar-Ruiz et al., 2024). Additionally, the broad and weak nature of this peak in the activated biochars (ABs) suggests their predominantly amorphous character (Choudhary et al., 2020). An increase in peak intensity following activation indicates structural enhancement and increased crystallinity of the biochars (Yağmur and Kaya, 2021).

The textural features of the biochars were comprehensively evaluated through nitrogen adsorption–desorption isotherm analysis. The resulting pore size distribution and adsorption isotherms are illustrated in Figures 3 and 4. According to IUPAC classification, the physisorption isotherms of all three H_3PO_4 activated biochars correspond to Type IV with an H4-type hysteresis loop observed at relative pressures (P/P_0) > 0.45, indicating the predominance of mesoporous structures (Ouyang et al., 2023). In contrast, the isotherm of the raw biochar is characteristic of a Type I profile, confirming its predominantly microporous nature, with a pore diameter of 1.47 nm and a low specific surface area of 32 m^2/g as reported in Table 3. These features suggest a limited and less accessible adsorption capacity due to the narrow pore size (Zhang et al., 2023). By comparison, the H_3PO_4 activated biochars (AB40, AB70, and AB100) exhibited significantly higher specific surface areas: 208 m^2.g^{-1}, 296 m^2.g^{-1} and 348 m^2.g^{-1}, respectively and a more developed pore structure. Consequently, methyl orange molecules were expected to be adsorbed not only onto the external surface but also within the internal pores of the activated biochars via a pore-filling mechanism (Jabar et al., 2022).

Adsorption studies

MO adsorption isotherm

Figure 5 illustrates how the equilibrium concentration (Qe = f[Ce]) affects the equilibrium adsorbed quantity. The findings suggest that the isotherm follows type L, as per the classification of Giles. The empirical Freundlich constants K_f and n are difficult to use. They respectively give an indication of the adsorption capacity and the intensity of the adsorption reaction. The coefficients

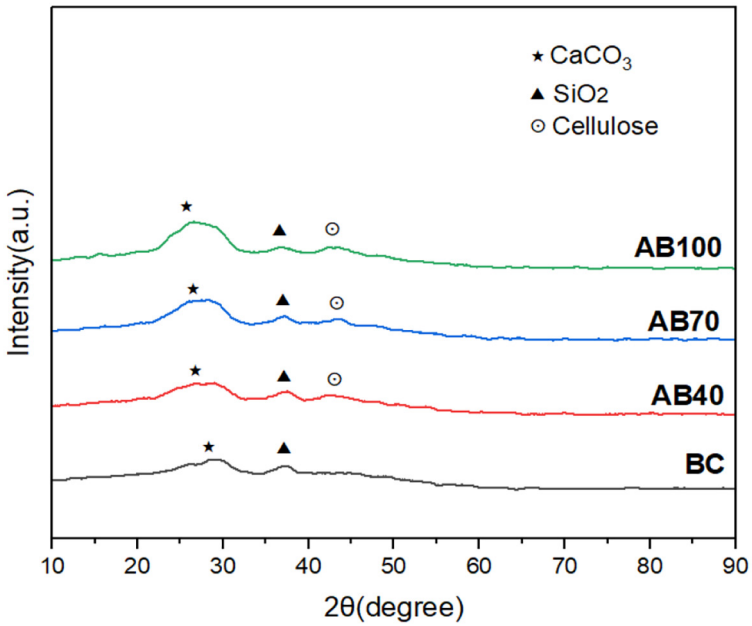

Figure 2. XRD patterns of biochars

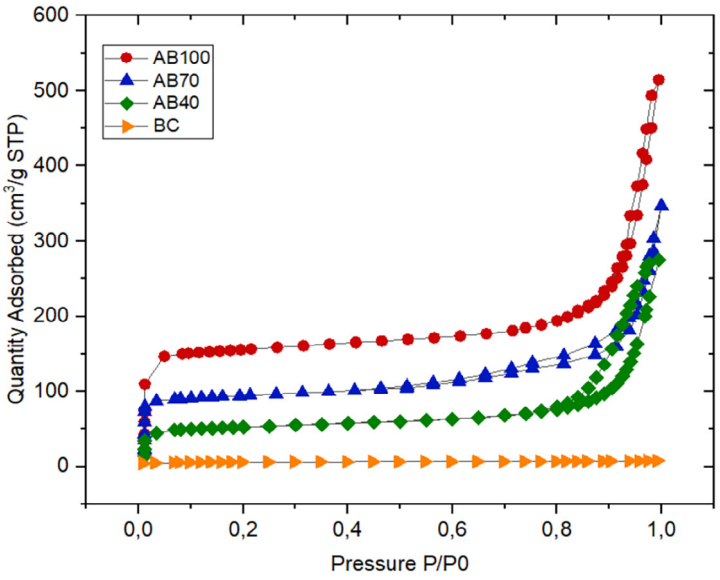

Figure 3. N_2 adsorption-desorption isotherms of the biochars

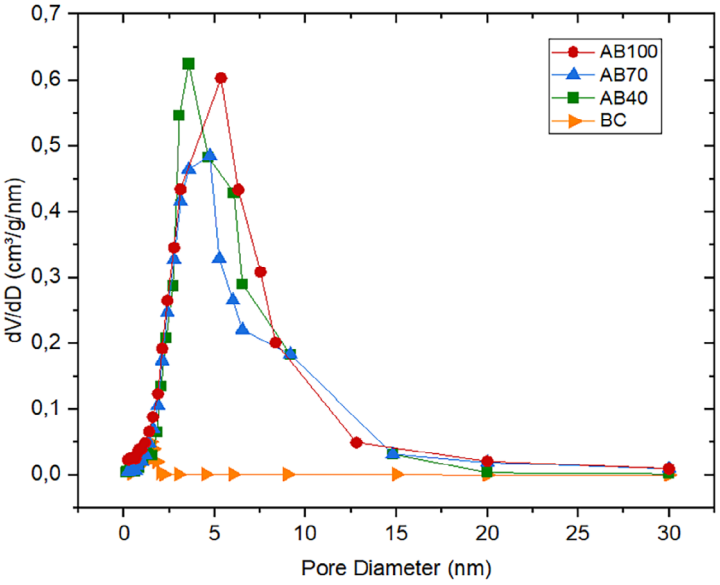

Figure 4. Pore size distribution for the biochars

Table 3. BET characteristics of BC and ABs

Biochar type	S_{BET} ($m^2.g^{-1}$)	D_p (nm)
AB40	208.2665	3.4
AB70	347.6402	4.7
AB100	395.8272	5.3
BC	32.936	1.47

of determination of the models studied presented in Table 4 indicate that the Langmuir model fits the dye adsorption process very well. The correlation coefficient values are 0.99 for all ABs. The maximum adsorbed quantities obtained by the Langmuir model for AB40, AB70, AB100 are equal to 71.83, 89.87 and 143.65 $mg \cdot g^{-1}$ respectively. The Langmuir separation factor values fall within the valid range (between 0 and 1). The Q_{max} values of the Langmuir model increase with increasing impregnation ratio, thus confirming that specific surface area increases as a function of impregnation ratio.

The parameter *n* of the Freundlich model, representing surface heterogeneity according to the literature, ranges from 0 to 1, which would mean that the adsorbent surface would present an increasingly

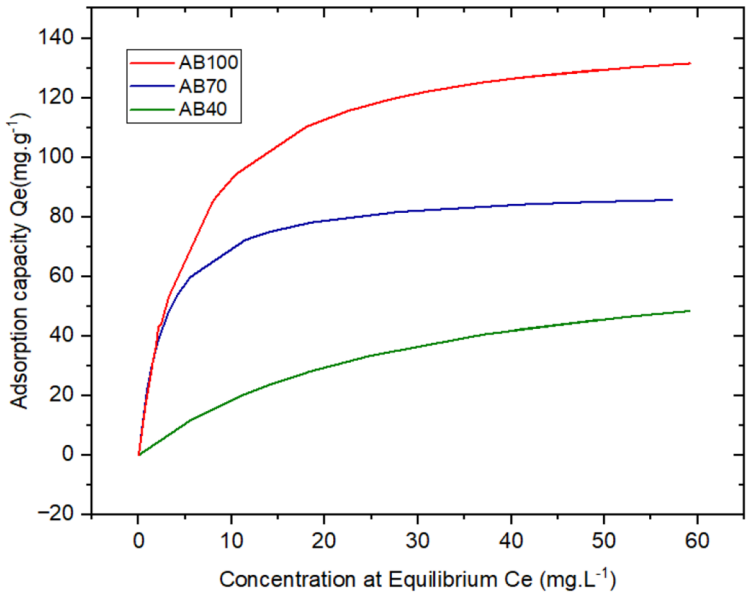

Figure 5. Adsorption isotherms of orange methyl by activated biochars

Table 4. Parameters of methylorange adsorption isotherms by activated biochars in Langmuir, Freundlish and Temkin models

Parameter	Biochar		
	AB40	AB70	AB100
Langmuir isotherm			
Q_{max} (mg. g^{-1})	71.83	89.87	143.65
K_L (L.mg^{-1})	0.03	0.35	0.18
R^2	0.99	0.99	0.99
Freundlish isotherm			
n	0.43	0.22	0.39
K_f	7.84	36.45	36.58
R^2	0.99	0.99	0.98
Temkin isotherm			
B (L.g^{-1})	14.96	15.53	27.29
A	7.02	5.40	4.39
R^2	0.94	0.97	0.97

heterogeneous texture for biochars in the following order: AB40 > AB70, AB100 (Zhao and Lang, 2018). When the Freundlich exponent $n > 1$, this indicates that the adsorbate is weakly bound to the adsorbent, which is characterized by a low variation in adsorption free energy. In this study, the exponent $n < 1$ would indicate a strong adsorbate-adsorbent interaction. The adsorption capacity of MO dye on biochars follows the following order: AB100 > AB70 > AB40 (Figure 5). The different adsorption capacities can be attributed to the different textures of these adsorbents. It is important to highlight that the Q_{max} capacity values derived from the Langmuir model and reported in previous studies are generally lower than those determined for AB100 in the present study as indicated in Table 5.

MO adsorption kinetics (contact time effect)

For the three ABs in this study, Figure 6 indicates that Q_{max}AB100 > Q_{max}AB70 > Q_{max}AB40 and that the contact time required to establish equilibrium is around 90 minutes (1h 30 min). This shows that adsorbent performance is linked to the impregnation ratio. The validity of the kinetic models is examined on the basis of the value of the linear

Table 5. Methyl orange adsorption capacity of AB100 activated biochar compared with the capacity of adsorbents documented in the literature

Adsorbent name	Q_{max} (mg. g^{-1})	Reference
Sulfactant-modified pineapple leaf	47.62	(Kamaru et al., 2016)
Biochar from chicken manure	41.49	(Yu et al., 2018)
Geothite	55	(Munagapati et al., 2017a)
Banana pseudo steam-based hydrogel	9.47	(Bello et al., 2018)
Cu_2O particles	96.42	(W. C. J. Ho et al., 2017)
Graphene oxide	16.83	(Robati et al., 2016)
Chitosan beads	84	(Munagapati et al., 2017b)
Activated carbon from coconut shell	3	(Islam et al., 2016)
Calcinated organic matter-rich clays from Egypt	34.48	(Zayed et al., 2018)
Biochar		
AB40	71.83	This study
AB70	89.87	
AB100	143.65	

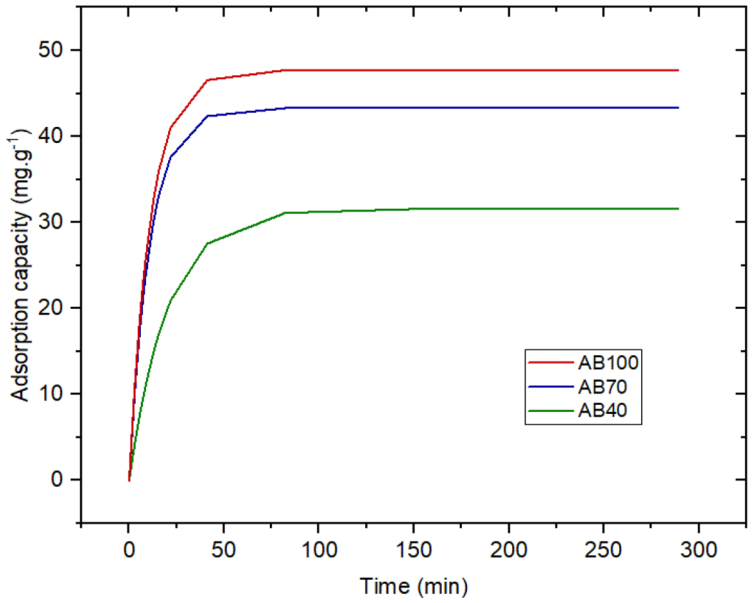

Figure 6. Methyl orange adsorption kinetics by activated biochars (ABs)

coefficient of determination R^2 and the calculated theoretical adsorbed quantities ($Q_{e,the}$) reported in Table 6. For the intraparticle diffusion model, the value of the coefficient of determination obtained is between 0.92 and 0.98, indicating a relatively low correlation. By contrast, application of the pseudo-first-order model leads to coefficients of determination of the order of 0.96. In contrast, the coefficients of determination of the pseudo-second-order kinetic model are between 0.98 and 0.99, and thus closer to 1 than for all other models. The values of $Q_{e,the}$ estimated by the first-order kinetic and intraparticle diffusion models (Table 6) differed from the experimental values. For the pseudo-second-order model, the value of the adsorption rate (h) increases with increasing impregnation ratio, and the values of adsorbed quantities $Q_{e,the}$ calculated by the pseudo-second-order model are comparable to the experimental values $Q_{e,exp}$. This shows that the adsorption kinetics are perfectly described by the pseudo-second-order kinetic model for the ABs studied (Figure 7). Kinetic analyses carried out by other researchers have also demonstrated that the pseudo-second-order model accurately describes the adsorption behavior of orange methyl dye on biochar (Yu et al., 2018).

Table 6. Parameters of the kinetic model of methyl orange adsorption by activated biochars

Parameter	Biochar		
	AB40	AB70	AB100
$Q_{e,exp}$ (mg.g^{-1})	31.10	43.31	47.72
Pseudo first order kinetics			
$Q_{e,the}$ (mg.g^{-1})	21.88	35.08	29 .68
K_1 (min^{-1})	0.011	0.013	0.018
R^2	0 .97	0.99	0.96
Pseudo second order kinetics			
$Q_{e,the}$ (mg.g^{-1})	34.88	45.08	49.28
K_2 (g.mg^{-1}.min^{-1})	0.001	0.002	0.002
R^2	0.98	0.99	0.99
Weber and Morris intraparticle diffusion			
$Q_{e,the}$ (mg.g^{-1})	17.12	28.98	31.48
K_{int}	2.17	2.49	2.70
C	4.60	14.62	15.88
R^2	0.98	0.92	0.94

According to Table 7, the findings demonstrated that adsorption capacity tends to rise as the temperature increases and the ΔH° values for the three types of biochar (AB40, AB70, AB100) are all positive (31.36 kJ/mol^{-1} to 35.70 kJ/mol^{-1}), suggesting that adsorption is endothermic in nature and the forces responsible for adsorption are mainly van der Waals along with π–π interactions (Nguyen et al., 2023). Moreover, entropy (ΔS°) is relatively high (around 51 to 52 kJ/mol^{-1}. K^{-1}), suggesting that the adsorption process may lead to increased disorder in the system (Chen et al., 2022). Finally, for all biochar types (AB40, AB70, AB100), ΔG° is positive and increases with temperature, indicating non-spontaneous adsorption and increasing energy dependence, respectively. Overall, the adsorption of methyl orange (MO) onto the activated biochars likely involves multiple mechanisms, including electrostatic attraction at low pH

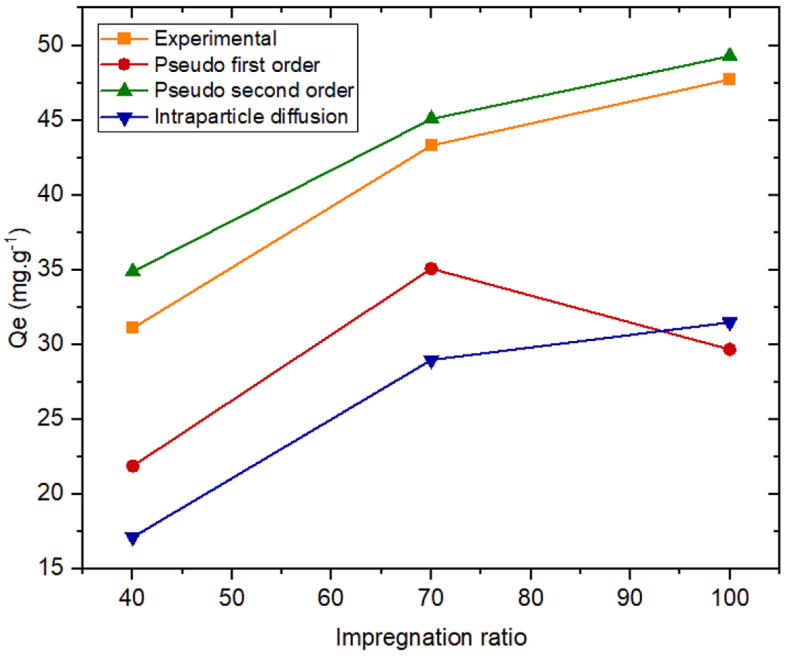

Figure 7. Experimental adsorption capacity of orange methyl by activated biochars compared with model-calculated adsorption capacities

Table 7. Thermodynamic characteristics of MO adsorption onto ABs

Biochar	△H° (KJ.mol$^{-1)}$	△S°	△G° (KJ.mol^{-1})		
		(KJ.mol^{-1}.K^{-1})	17°C	25°C	45°C
AB40	31.36	51.27	16.48	16.07	15.05
AB70	32.51	51.78	17.49	17.07	16.04
AB100	35.70	52.42	20.49	20.07	19.02

between the protonated biochar surface and the anionic sulfonate groups of MO, π–π stacking interactions arising from their aromatic structures, and hydrogen bonding between MO and surface functional groups (Chen et al., 2020). Furthermore, the porous structure of the activated biochars may facilitate dye retention through a pore-filling mechanism (Lu et al., 2021).

CONCLUSIONS

This study demonstrates that biochar derived from *Malus domestica* debris, when activated with phosphoric acid, serves as an efficient adsorbent for the elimination of methyl orange (MO) from aqueous solutions. The physicochemical characterization of the activated biochar revealed a high specific surface area (348 $m^2 \cdot g^{-1}$) and an iodine index of 363 $mg \cdot g^{-1}$, indicating well-developed porosity conducive to adsorption. Additionally, the point of zero charge (pHpzc) values of the majority of biochars were below 7, confirming their slightly acidic surface nature, which can influence adsorption interactions. Chemical analysis using Boehm titration demonstrated that phosphoric acid activation enhances the presence of functional groups, predominantly phenolic and carboxyl groups, which contribute to the adsorption mechanism. Equilibrium adsorption studies confirmed that the Langmuir isotherm model best describes the adsorption process, suggesting monolayer adsorption onto homogeneous active sites. Furthermore, based on the experimental results, equilibrium adsorption kinetics followed a pseudo-second-order model and the thermodynamic analysis indicated that adsorption is endothermic and primarily governed by physical interactions, with increasing temperature favoring MO uptake. The adsorption of methyl orange onto activated biochars involves electrostatic attraction and π–π interactions. The porous structure also promotes dye retention through a pore-filling effect. These findings emphasize the significant potential of Malus domestica-derived biochar as a sustainable, cost-effective alternative for dye removal from wastewater, offering a viable solution to mitigate water pollution. Future research should explore its performance in real wastewater treatment applications and investigate its adsorption efficiency for a broader range of organic pollutants.

Acknowledgments

The authors gratefully acknowledge the farmers of Dayet Aoua Ifrane for collecting the raw material and the innovation center of Moulay Abdellah Fes University for helping with the characterization tests.

REFERENCES

1. Alcazar-Ruiz, A., Maisano, S., Chiodo, V., Urbani, F., Dorado, F., Sanchez-Silva, L. (2024). Enhancing CO2 capture performance through activation of olive pomace biochar: A comparative study of physical and chemical methods. *Sustainable Materials and Technologies*, *42*. https://doi.org/10.1016/j.susmat.2024.e01177
2. Biswal, B. K., Balasubramanian, R. (2023). Use of biochar as a low-cost adsorbent for removal of heavy metals from water and wastewater: A review. *Journal of Environmental Chemical Engineering*, *11*(5). https://doi.org/10.1016/j.jece.2023.110986
3. Boumanchar, I., Chhiti, Y., M'hamdi Alaoui, F. E., El Ouinani, A., Sahibed-Dine, A., Bentiss, F., Jama, C., Bensitel, M. (2017). Effect of materials mixture on the higher heating value: Case of biomass, biochar and municipal solid waste. *Waste Management*, *61*, 78–86. https://doi.org/10.1016/j.wasman.2016.11.012
4. Candamano, S., Coppola, G., Mazza, A., Caicho Caranqui, J. I., Bhattacharyya, S., Chakraborty, S., Alexis, F., Algieri, C. (2023). Batch and fixed bed adsorption of methylene blue onto foamed metakaolin-based geopolymer: A preliminary investigation. *Chemical Engineering Research and Design*, *197*, 761–773. https://doi.org/10.1016/j.cherd.2023.08.014
5. Chen, K., Ma, D., Yu, H., Zhang, S., Seyler, B. C., Chai, Z., Peng, S. (2022). Biosorption of V(V) onto Lantana camara biochar modified by H3PO4: Characteristics, mechanism, and regenerative capacity. *Chemosphere*, *291*. https://doi.org/10.1016/j.chemosphere.2021.132721
6. Chen, M., He, F., Hu, D., Bao, C., Huang, Q. (2020). Broadened operating pH range for adsorption/reduction of aqueous Cr(VI) using biochar from directly treated jute (*Corchorus capsularis* L.) fibers by H3PO4. *Chemical Engineering Journal*, *381*. https://doi.org/10.1016/j.cej.2019.122739
7. Choudhary, M., Kumar, R., Neogi, S. (2020). Activated biochar derived from *Opuntia ficus-indica* for the efficient adsorption of malachite green dye, Cu+2 and Ni+2 from water. *Journal of Hazardous Materials*, *392*. https://doi.org/10.1016/j.jhazmat.2020.122441

8. Chu, G., Zhao, J., Huang, Y., Zhou, D., Liu, Y., Wu, M., Peng, H., Zhao, Q., Pan, B., Steinberg, C. E. W. (2018). Phosphoric acid pretreatment enhances the specific surface areas of biochars by generation of micropores. *Environmental Pollution*, *240*, 1–9. https://doi.org/10.1016/j.envpol.2018.04.003
9. Dai, L., Lu, Q., Zhou, H., Shen, F., Liu, Z., Zhu, W., Huang, H. (2021). Tuning oxygenated functional groups on biochar for water pollution control: A critical review. In *Journal of Hazardous Materials* 420. Elsevier B.V. https://doi.org/10.1016/j.jhazmat.2021.126547
10. Dutta, D., Arya, S., Kumar, S. (2021). Industrial wastewater treatment: Current trends, bottlenecks, and best practices. *Chemosphere*, *285*. https://doi.org/10.1016/j.chemosphere.2021.131245
11. El Alouani, M., Alehyen, S., El Achouri, M., Taibi, M. (2018). Adsorption of cationic dye onto fly ash-based geopolymer: Batch and fixed bed column studies. *MATEC Web of Conferences*, *149*, 02088. https://doi.org/10.1051/matecconf/201814902088
12. Fikri, N., Hattafi, Y., Mardi, L., El Amarty, F., El Hassani, F., Benaabidate, L., Lahrach, A. (2025). Production and application of biochar: A bibliometric-bibliographic study from 2004 to 2023. *Journal of Environmental Engineering and Science*. https://doi.org/10.1680/jenes.24.00107
13. Ighalo, J. O., Omoarukhe, F. O., Ojukwu, V. E., Iwuozor, K. O., Igwegbe, C. A. (2022). Cost of adsorbent preparation and usage in wastewater treatment: A review. *Cleaner Chemical Engineering*, *3*, 100042. https://doi.org/10.1016/j.clce.2022.100042
14. Iwuozor, K. O., Ighalo, J. O., Emenike, E. C., Ogunfowora, L. A., Igwegbe, C. A. (2021). Adsorption of methyl orange: A review on adsorbent performance. *Current Research in Green and Sustainable Chemistry*, *4*. https://doi.org/10.1016/j.crgsc.2021.100179
15. Jabar, J. M., Odusote, Y. A., Ayinde, Y. T., Yılmaz, M. (2022). African almond (*Terminalia catappa* L) leaves biochar prepared through pyrolysis using H_3PO_4 as chemical activator for sequestration of methylene blue dye. *Results in Engineering*, *14*. https://doi.org/10.1016/j.rineng.2022.100385
16. Jiang, H., Li, X., Dai, Y. (2024). Phosphoric acid activation of cow dung biochar for adsorbing enrofloxacin in water: Icing on the cake. *Environmental Pollution*, *341*. https://doi.org/10.1016/j.envpol.2023.122887
17. Kim, Y., Ok, J. I., Vithanage, M., Park, Y. K., Lee, J., Kwon, E. E. (2019). Modification of biochar properties using CO2. *Chemical Engineering Journal*, *372*, 383–389. https://doi.org/10.1016/j.cej.2019.04.170
18. Kozyatnyk, I., Oesterle, P., Wurzer, C., Mašek, O., Jansson, S. (2021). Removal of contaminants of emerging concern from multicomponent systems using carbon dioxide activated biochar from lignocellulosic feedstocks. *Bioresource Technology*, *340*. https://doi.org/10.1016/j.biortech.2021.125561
19. Lellis, B., Fávaro-Polonio, C. Z., Pamphile, J. A., Polonio, J. C. (2019). Effects of textile dyes on health and the environment and bioremediation potential of living organisms. *Biotechnology Research and Innovation*, *3*(2), 275–290. https://doi.org/10.1016/j.biori.2019.09.001
20. Lu, Z., Zhang, H., Shahab, A., Zhang, K., Zeng, H., Bacha, A. U. R., Nabi, I., Ullah, H. (2021). Comparative study on characterization and adsorption properties of phosphoric acid activated biochar and nitrogen-containing modified biochar employing Eucalyptus as a precursor. *Journal of Cleaner Production*, *303*. https://doi.org/10.1016/j.jclepro.2021.127046
21. Nguyen, T. K. T., Nguyen, T. B., Chen, W. H., Chen, C. W., Kumar Patel, A., Bui, X. T., Chen, L., Singhania, R. R., Dong, C. Di. (2023). Phosphoric acid-activated biochar derived from sunflower seed husk: Selective antibiotic adsorption behavior and mechanism. *Bioresource Technology*, *371*. https://doi.org/10.1016/j.biortech.2023.128593
22. Ouyang, J., Chen, J., Chen, W., Zhou, L., Cai, D., Ren, C. (2023). H_3PO_4 activated biochars derived from different agricultural biomasses for the removal of ciprofloxacin from aqueous solution. *Particuology*, *75*, 217–227. https://doi.org/10.1016/j.partic.2022.07.016
23. Premchand, P., Demichelis, F., Galletti, C., Chiaramonti, D., Bensaid, S., Antunes, E., Fino, D. (2024). Enhancing biochar production: A technical analysis of the combined influence of chemical activation (KOH and NaOH) and pyrolysis atmospheres (N_2/CO_2) on yields and properties of rice husk-derived biochar. *Journal of Environmental Management*, *370*. https://doi.org/10.1016/j.jenvman.2024.123034
24. Saadatkhah, N., Carillo Garcia, A., Ackermann, S., Leclerc, P., Latifi, M., Samih, S., Patience, G. S., Chaouki, J. (2020). Experimental methods in chemical engineering: Thermogravimetric analysis—TGA. In *Canadian Journal of Chemical Engineering* 98(1), 34–43. Wiley-Liss Inc. https://doi.org/10.1002/cjce.23673
25. Shao, J., Zhang, J., Zhang, X., Feng, Y., Zhang, H., Zhang, S., Chen, H. (2018). Enhance SO2 adsorption performance of biochar modified by CO2 activation and amine impregnation. *Fuel*, *224*, 138–146. https://doi.org/10.1016/j.fuel.2018.03.064
26. Sudarshan, S., Harikrishnan, S., RathiBhuvaneswari, G., Alamelu, V., Aanand, S., Rajasekar, A., Govarthanan, M. (2023). Impact of textile dyes on human health and bioremediation of textile industry effluent using microorganisms: current status and future prospects. In *Journal of Applied*

Microbiology 134(2). Oxford University Press. https://doi.org/10.1093/jambio/lxac064

27. Usman, A. R. A., Abduljabbar, A., Vithanage, M., Ok, Y. S., Ahmad, M., Ahmad, M., Elfaki, J., Abdulazeem, S. S., Al-Wabel, M. I. (2015). Biochar production from date palm waste: Charring temperature induced changes in composition and surface chemistry. *Journal of Analytical and Applied Pyrolysis*, *115*, 392–400. https://doi.org/10.1016/j.jaap.2015.08.016
28. Wang, L., Ok, Y. S., Tsang, D. C. W., Alessi, D. S., Rinklebe, J., Wang, H., Mašek, O., Hou, R., O'Connor, D., Hou, D. (2020). New trends in biochar pyrolysis and modification strategies: feedstock, pyrolysis conditions, sustainability concerns and implications for soil amendment. In *Soil Use and Management* 36(3), 358–386. Blackwell Publishing Ltd. https://doi.org/10.1111/sum.12592
29. Yağmur, H. K., Kaya, İ. (2021). Synthesis and characterization of magnetic $ZnCl_2$-activated carbon produced from coconut shell for the adsorption of methylene blue. *Journal of Molecular Structure*, *1232*. https://doi.org/10.1016/j.molstruc.2021.130071
30. Yu, J., Zhang, X., Wang, D., Li, P. (2018). Adsorption of methyl orange dye onto biochar adsorbent prepared from chicken manure. *Water Science and Technology*, *77*(5), 1303–1312. https://doi.org/10.2166/wst.2018.003
31. Zeng, H., Zeng, H., Zhang, H., Shahab, A., Zhang, K., Lu, Y., Nabi, I., Naseem, F., Ullah, H. (2021). Efficient adsorption of Cr (VI) from aqueous environments by phosphoric acid activated eucalyptus biochar. *Journal of Cleaner Production*, *286*. https://doi.org/10.1016/j.jclepro.2020.124964
32. Zhang, Y., Shen, B., Sajjad Ahmad, M., Zhou, W., Khalid, R. R., Ibrahim, M., Bokhari, A. (2023). A three-dimensional active biochar for sintering in steel industry and remove methylene blue by synergistic activation of H_3PO_4 and $ZnCl_2$. *Fuel*, *336*. https://doi.org/10.1016/j.fuel.2022.127079
33. Zhao, H., Lang, Y. (2018). Adsorption behaviors and mechanisms of florfenicol by magnetic functionalized biochar and reed biochar. *Journal of the Taiwan Institute of Chemical Engineers*, *88*, 152–160. https://doi.org/10.1016/j.jtice.2018.03.049